Adiabatic-nuclei calculations of positron scattering from molecular hydrogen

Mark C. Zammit,[1,2,*] Dmitry V. Fursa,[2] Jeremy S. Savage,[2] Igor Bray,[2] Luca Chiari,[3] Antonio Zecca,[4] and Michael J. Brunger[5]

[1]*Theoretical Division, Los Alamos National Laboratory, Los Alamos, New Mexico 87545, USA*

[2]*Curtin Institute for Computation and Department of Physics, Astronomy and Medical Radiation Sciences, Curtin University, Perth, Western Australia 6102, Australia*

[3]*Department of Physics, Tokyo University of Science, 1-3 Kagurazaka, Shinjuku, Tokyo 162-8601, Japan*

[4]*Department of Physics, University of Trento, Via Sommarive 14, Povo, Trento 38123, Italy*

[5]*School of Chemical and Physical Sciences, Flinders University, GPO Box 2100, Adelaide, South Australia 5001, Australia*

(Received 14 November 2016; published 6 February 2017)

The single-center adiabatic-nuclei convergent close-coupling method is used to investigate positron collisions with molecular hydrogen (H_2) in the ground and first vibrationally excited states. Cross sections are presented over the energy range from 1 to 1000 eV for elastic scattering, vibrational excitation, total ionization, and the grand total cross section. The present adiabatic-nuclei positron-H_2 scattering length is calculated as $A = -2.70a_0$ for the ground state and $A = -3.16a_0$ for the first vibrationally excited state. The present elastic differential cross sections are also used to "correct" the low-energy grand total cross-section measurements of the Trento group [A. Zecca *et al.*, Phys. Rev. A **80**, 032702 (2009)] for the forward-angle-scattering effect. In general, the comparison with experiment is good. By performing convergence studies, we estimate that our $R_m = 1.448a_0$ fixed-nuclei results are converged to within $\pm 5\%$ for the major scattering integrated cross sections.

DOI: 10.1103/PhysRevA.95.022707

I. INTRODUCTION

Positron scattering from molecular hydrogen (H_2) is a natural testing ground for both theoretical and experimental studies of collision physics and transport modeling [1,2], which underpins several areas of technological and scientific research. Of particular interest is to quantify the radiation damage associated with positron thermalization [1–3] and the subsequent secondary species [4,5] in positron emission tomography scans. Our focus on H_2 is the foundation for molecules of biological relevance.

Another area of active research is to determine the source of positrons in the Milky Way galaxy, where over the past 40 years positron-annihilation radiation has been detected from various directions of the galaxy. In particular, in the central region of our galaxy $\approx 10^{43}$ positrons are produced per second [6]. Given that H_2 is the most abundant molecule in interstellar space, studies of positron collisions with H_2 are particularly important in modeling positron propagation through the interstellar medium [6].

Positron-H_2 scattering experiments have measured the grand total cross section (GTCS) [7–13], direct ionization cross section (DICS) [14–16], positronium (Ps) formation cross section [10,13,14], total ionization cross section (TICS) [14,17], electronic $X\,^1\Sigma_g^+ \rightarrow B\,^1\Sigma_u^+$ excitation cross section [18,19], vibrational $0 \rightarrow 1$ excitation cross section [19], elastic integrated cross section, and low-energy elastic differential cross section (DCS) [13]. Measurements of the GTCS vary greatly in the low-energy region. These variations are primarily due to different experimental resolution of scattering to forward angles [12,13,20]. Theoretical results have been used to "correct" the low-energy measurements of the integrated cross sections for this forward-scattering effect [13,20–22].

Theoretical studies of the positron-molecule scattering problem present a range of complexities. These include the multicenter nature of the problem, the difficulty of accounting for the Ps-formation channel, and the molecular electronic, vibrational, and rotational degrees of freedom. In addition, the positron-electron interaction is strongly correlated [23] and needs to be treated accurately at relatively large distances. The two-center close-coupling method (which includes the positronium formation channels explicitly) is the most consistent way to account for long-range positron-electron correlations. The pioneering work of Hewitt *et al.* [24,25], Higgins and Burke [26], Mitroy [27], and Walters *et al.* [28] demonstrated the success of using two-center expansions consisting of Ps and atomic states. The two-center approach has also been utilized within the convergent close-coupling (CCC) method for positron-atom scattering [29–31] and recently for positron-H_2 scattering [32]. This work was recently reviewed in Refs. [33,34]. To date, the only other two-center coupled-channel positron-molecule (H_2) calculations were conducted by Biswas *et al.* [35], which only included the ground states of H_2 and Ps. However, the two-centre approach is computationally demanding and relatively complicated to implement.

Alternatively, the single-center approach (close-coupling expansion over the target space) can be applied to positron scattering. This method is significantly simpler to implement than the two-center approach and is found to be computationally very stable. In the single-center expansion method the long-range correlations of the positron-electron potential can be described by a relatively large partial-wave expansion of the potential. These large partial waves are constructed from one-electron orbitals that have large orbital angular momentum. In addition, coupling positive-energy target pseudostates collectively takes into account electron loss, which includes both the direct ionization and Ps-formation channels. This method is capable of obtaining reliable results for energies outside the small energy region between the Ps-formation and ionization thresholds [36]. For positron-H_2 scattering this

*mzammit@lanl.gov

method has been used extensively by coupled-channel methods, which include the molecular R matrix with pseudostates (MRMPS) [37], Schwinger multichannel (SMC) [38,39], and complex Kohn variational [40] methods. These multichannel calculations have traditionally focused on the low-energy region. In general, these methods are in good agreement with old experiments in the energy range from 0 to 10 eV for the GTCS [8,41], however they considerably underestimate the most recent measurements of Karwasz *et al.* [11], Zecca *et al.* [12], and Machacek *et al.* [13].

Following Zammit *et al.* [42], which presented the single-center CCC method and fixed-nuclei results for positron-H_2 scattering, we provide details of the method and explicitly demonstrate convergence of the fixed-nuclei results. Calculations are performed within the fixed-nuclei and adiabatic-nuclei approximations. The latter is used to verify the accuracy of the fixed-nuclei calculations and to model scattering from the $v_i = 0$ ground state and the $v_i = 1$ first excited vibrational state. Results are presented for the scattering length, GTCS, TICS, vibrational excitation integrated cross section, elastic integrated cross section, and elastic DCS.

II. METHOD

The CCC method is formulated in a spherical coordinate system where the origin is set at the midpoint between the two nuclei and the z axis is chosen to align along the internuclear axis $\boldsymbol{R}$ (body frame). Atomic units are used throughout the paper unless specifically indicated.

A. Target states

The H_2 target electronic Hamiltonian $H_{\rm T}^{\rm elec}$ in the Born-Oppenheimer approximation describes two electrons in the Coulomb potential of two protons that are fixed at a distance R and is defined as

$$H_{\rm T}^{\rm elec} = H_1^{\rm elec} + H_2^{\rm elec} + V_{12} + 1/R, \tag{1}$$

where $1/R$ is the internuclear Coulomb repulsion term. The one-electron (or positron) electronic Hamiltonian $H_i^{\rm elec}$ is

$$H_i^{\rm elec} = K_i(r_i) + V_i(\boldsymbol{r}_i;\boldsymbol{R}), \tag{2}$$

where

$$K_i(r_i) = -\frac{1}{2}\frac{d^2}{dr_i^2} + \frac{l(l+1)}{2r_i^2}, \tag{3}$$

$$V_i(\boldsymbol{r}_i;\boldsymbol{R}) = \left(\frac{z_{\rm e}}{\left|\boldsymbol{r}_i + \frac{\boldsymbol{R}}{2}\right|} + \frac{z_{\rm e}}{\left|\boldsymbol{r}_i - \frac{\boldsymbol{R}}{2}\right|}\right), \tag{4}$$

and $z_{\rm e} = -1$ for the charge of an electron or $z_{\rm e} = 1$ for the charge of a positron. The fixed-nuclei electron-nuclei (or positron-nuclei) potential (4) is expanded in partial waves

$$V_i(\boldsymbol{r}_i;\boldsymbol{R}) = 2z_{\rm e}\sum_{\lambda=0,2,4,\ldots}^{\infty}\sqrt{\frac{4\pi}{(2\lambda+1)}}v_\lambda(r_i,R/2)Y_{\lambda 0}(\hat{\boldsymbol{r}}_i), \tag{5}$$

where $v_\lambda(r_i,r_j) = r_<^\lambda/r_>^{\lambda+1}$, $r_< = \min(r_i,r_j)$, and $r_> = \max(r_i,r_j)$. Here V_{12} is the electron-electron (or positron-electron) potential and is expanded in partial waves

$$\begin{aligned} V_{i,j} &= -\frac{z_{\rm e}}{|\boldsymbol{r}_i - \boldsymbol{r}_j|} \\ &= -z_{\rm e}\sum_{\lambda\mu}^{\infty}(-1)^\mu\frac{4\pi}{(2\lambda+1)} \\ &\quad\times v_\lambda(r_i,r_j)Y_{\lambda-\mu}(\hat{\boldsymbol{r}}_i)Y_{\lambda\mu}(\hat{\boldsymbol{r}}_j). \end{aligned} \tag{6}$$

H_2 electronic target states are characterized by their orbital angular momentum projection m, parity π, and spin s. The target Hamiltonian (1) is diagonalized for each (m, π, s) term in a set of antisymmetrized two-electron configurations $\phi^{m\pi s}(\mathbf{x}_1,\mathbf{x}_2)$,

$$\begin{aligned} \phi_{\gamma,\delta}^{m\pi s}(\mathbf{x}_1,\mathbf{x}_2) &= \frac{1}{\sqrt{2(1+\delta_{\gamma,\delta})}}\mathcal{A} \\ &\quad\times|\phi_\gamma(\mathbf{x}_1)\phi_\delta(\mathbf{x}_2) : m\pi s m_s\rangle, \end{aligned} \tag{7}$$

where $\mathbf{x}$ is used to denote both the spin and spatial coordinates and the antisymmetrization operator $\mathcal{A} = 1 - P_{12}$. The one-electron orbitals $\phi(\mathbf{x})$,

$$\phi_j^{m'\pi'}(\mathbf{x}) = \frac{1}{r}\varphi_{k_j l_j}(r)Y_{l_j m_j}(\hat{\boldsymbol{r}})\chi_{m_{s_j}}(\sigma), \tag{8}$$

are represented by Laguerre basis functions with $m_j = m'$, $(-1)^{l_j} = \pi'$, and $\chi_{m_{s_j}}(\sigma)$ is the spin-$\frac{1}{2}$ eigenfunction with angular projection m_{s_j}. These Laguerre basis functions have the form

$$\begin{aligned} \varphi_{kl}(r) &= \sqrt{\frac{\alpha_l(k-1)!}{(k+l)(k+2l)!}}(2\alpha_l r)^{l+1} \\ &\quad\times\exp(-\alpha_l r)L_{k-1}^{2l+1}(2\alpha_l r), \end{aligned} \tag{9}$$

where α_l is the exponential falloff parameter, L_{k-1}^{2l+1} are the associated Laguerre polynomials of order $2l+1$, and k ranges from 1 to N_l. We designate N_l as the number of Laguerre basis functions per orbital angular momentum l up to $l_{\rm max}$. Matrix elements of the target Hamiltonian are evaluated analytically utilizing properties of the Laguerre basis functions [43].

Upon diagonalization of the H_2 target Hamiltonian (1), configuration-interaction (CI) coefficients $C_{\gamma,\delta}^{(n)}$ and eigenvalues are obtained. For brevity of notation, the H_2 two-electron target states are represented by ordered configurations

$$\begin{aligned} \Phi_n^{m\pi s}(\mathbf{x}_1,\mathbf{x}_2) &= \sum_{\gamma\delta}C_{\gamma,\delta}^{(n)}|\phi_\gamma(\mathbf{x}_1)\phi_\delta(\mathbf{x}_2) : m\pi s m_s\rangle \\ &= \frac{1}{r_1 r_2}\sum_{\gamma\delta}C_{\gamma,\delta}^{(n)}\varphi_\gamma(r_1)\varphi_\delta(r_2) \\ &\quad\times Y_{l_\gamma m_\gamma}(\hat{\boldsymbol{r}}_1)Y_{l_\delta m_\delta}(\hat{\boldsymbol{r}}_2)X_{m_s}^s, \end{aligned} \tag{10}$$

where, to account for the antisymmetry of the two-electron wave functions (10), the CI coefficients satisfy $C_{\gamma\delta}^{(n)} = (-1)^s C_{\delta\gamma}^{(n)}$ and

$$X_{m_s}^s = \sum_{m_{s_\gamma}m_{s_\delta}}C_{\frac{1}{2}m_{s_\gamma},\frac{1}{2}m_{s_\delta}}^{sm_s}\chi_{m_{s_\gamma}}(\sigma_1)\chi_{m_{s_\delta}}(\sigma_2). \tag{11}$$

It is important to note that as in the case of H_2^+ [44,45], the single-center Laguerre basis expansion of H_2 leads to slow

convergence with respect to the orbital angular momentum l of the basis, in particular, for the $X\,^1\Sigma_g{}^+$ ground state. To improve accuracy and save on computational resources, structure calculations are performed in two steps. First, a large Laguerre basis is used to diagonalize the $H_2{}^+$ target Hamiltonian and generate an accurate $1s\sigma_g$ state of $H_2{}^+$. Second, a new (smaller) Laguerre basis is produced. The $1s\sigma_g$ orbital of this new basis is replaced by the accurate $1s\sigma_g$ state calculated at the first step. This new basis is then used to construct the antisymmetrized two-electron configurations and diagonalize the H_2 target Hamiltonian (1).

B. Single-center CCC method

This work utilizes the molecular CCC formalism [45,46] to model positron-H_2 scattering within the single-center close-coupling expansion technique. Here the dependence on R is omitted from the notation unless it is explicitly indicated. In the positron single-center expansion method the total scattering wave function is expanded in terms of the target (H_2) pseudostates

$$\Psi_i^{SN(+)}(\mathbf{x}_0,\mathbf{x}_1,\mathbf{x}_2) = \sum_{n=1}^{N} f_{ni}^{SN(+)}(\mathbf{x}_0)\Phi_n^N(\mathbf{x}_1,\mathbf{x}_2) \equiv \left|\psi_i^{SN(+)}\right\rangle, \tag{12}$$

where S is the total electron and positron spin of the system, N is the total number of pseudostates included in the close-coupling expansion, $(+)$ denotes outgoing spherical-wave boundary conditions, and i denotes the initial state of the system. For positron scattering from the electronic ground state of H_2, the close-coupling expansion (12) contains only singlet states of H_2 and leads to total spin $S = 1/2$. The expansion in Eq. (12) includes Ps formation implicitly by including configurations that have an electron and positron in the continuum, which corresponds to both the direct ionization and Ps-formation channels. Hence the single-center expansion includes these channels indirectly and as a result the total ionization cross section (sum of the direct ionization and Ps-formation cross sections) can be calculated by summing over individual excitation cross sections to positive-energy pseudostates.

In the molecular CCC method we start with the body-frame scattering system Schrödinger equation for a fixed internuclear distance R,

$$(E^{(+)} - H)\left|\Psi_i^{SN(+)}\right\rangle = 0, \tag{13}$$

where E is the total energy of the scattering system. Ignoring the kinetic energy of the nuclei (fixed-nuclei approximation), the scattering system Hamiltonian H is defined as

$$H = H_{\rm T}^{\rm elec} + H_0^{\rm elec} + V_{01} + V_{02}, \tag{14}$$

where the index 0 denotes the projectile coordinate space and $H_0^{\rm elec}$ refers to the positron Hamiltonian given by Eq. (2).

The scattering system asymptotic Hamiltonian $H_{\rm asy}$ is chosen as

$$H_{\rm asy} = H_{\rm T}^{\rm elec} + K_0 + U_0, \tag{15}$$

where U_0 is an optional short-range distorting potential. Details of the short-range distorting potential U_0 will be given later. For this choice of $H_{\rm asy}$ the interaction potential (known as the direct term) is

$$V_U^{\rm D} = V_0 + V_{01} + V_{02} - U_0 = V_0 + 2V_{01} - U_0, \tag{16}$$

where the form in Eq. (16) is obtained by using the antisymmetrization property of the target states.

The CCC method utilizes the Green's function approach to transform the Schrödinger equation (13) to the momentum-space Lippmann-Schwinger equation

$$\left|\psi_i^{SN(+)}\right\rangle = \left|\Phi_i^N \boldsymbol{k}_i^{(+)}\right\rangle + \sum_{n=1}^{N} \sum\!\!\!\!\!\!\int_k d^3k \frac{\left|\Phi_n^N \boldsymbol{k}^{(-)}\right\rangle\left\langle \boldsymbol{k}^{(-)}\Phi_n^N\right|V_U^{\rm D}\left|\psi_i^{SN(+)}\right\rangle}{E^{(+)} - \varepsilon_k - \varepsilon_n^N + i0}. \tag{17}$$

Premultiplying Eq. (17) by $\langle \boldsymbol{k}_f^{(-)}\Phi_f^N|V_U^{\rm D}$, the coupled Lippmann-Schwinger equation for the distorted-wave T matrix is obtained

$$\left\langle \boldsymbol{k}_f^{(-)}\Phi_f^N\right|T_U^{SN}\left|\Phi_i^N \boldsymbol{k}_i^{(+)}\right\rangle = \left\langle \boldsymbol{k}_f^{(-)}\Phi_f^N\right|V_U^{\rm D}\left|\Phi_i^N \boldsymbol{k}_i^{(+)}\right\rangle + \sum_{n=1}^{N} \sum\!\!\!\!\!\!\int_k d^3k \frac{\left\langle \boldsymbol{k}_f^{(-)}\Phi_f^N\right|V_U^{\rm D}\left|\Phi_n^N \boldsymbol{k}^{(-)}\right\rangle\left\langle \boldsymbol{k}^{(-)}\Phi_n^N\right|T_U^{SN}\left|\Phi_i^N \boldsymbol{k}_i^{(+)}\right\rangle}{E^{(+)} - \varepsilon_k - \varepsilon_n^N + i0}, \tag{18}$$

where $\langle \boldsymbol{k}_f^{(-)}\Phi_f^N|T_U^{SN}|\Phi_i^N \boldsymbol{k}_i^{(+)}\rangle \equiv \langle \boldsymbol{k}_f^{(-)}\Phi_f^N|V_U^{\rm D}|\psi_i^{SN(+)}\rangle$. To solve Eq. (18), projectile distorted-wave functions $|\boldsymbol{k}^{(\pm)}\rangle$ are expanded in partial waves. The partial-wave expansion of the V (or T) matrix for an incident positron with linear momentum k_i, orbital angular momentum L_i, and orbital angular projection M_i has the form

$$\left\langle \boldsymbol{k}_f^{(-)}\Phi_f^N\right|V_U^{\rm D}\left|\Phi_i^N \boldsymbol{k}_i^{(\pm)}\right\rangle = (k_f k_i)^{-1} \sum_{\substack{L_f,L_i\\ M_f,M_i}} i^{L_i - L_f} e^{i(\delta_{L_f} \pm \delta_{L_i})} V_{fL_fM_f,iL_iM_i}^{\bar{M}\Pi S}(k_f,k_i) Y_{L_fM_f}\left(\hat{\boldsymbol{k}}_f^{(\rm b)}\right) Y_{L_iM_i}^*\left(\hat{\boldsymbol{k}}_i^{(\rm b)}\right). \tag{19}$$

For homonuclear diatomic molecules such as H_2 the projectile partial-wave expansion allows one to solve the Lippmann-Schwinger equations per partial wave of total orbital angular momentum projection $\bar{M} = M_i + m_i = M_f + m_f$, total parity $\Pi = (-1)^{L_i}\pi_i = (-1)^{L_f}\pi_f$, and total spin S.

The distorted-wave T matrix $\langle \boldsymbol{k}_f^{(-)} \Phi_f^N | T_U^{SN} | \Phi_i^N \boldsymbol{k}_i^{(+)} \rangle$ in Eq. (18) is solved via a K-matrix formulation, which enforces unitarity. After obtaining K-matrix elements and subsequently distorted-wave T-matrix elements, the physical T-matrix elements ($U_0 = 0$) are extracted from the distorted-wave T-matrix elements via

$$\langle \boldsymbol{q}_f \Phi_f^N | T^{SN} | \Phi_i^N \boldsymbol{q}_i \rangle = \langle \boldsymbol{k}_f^{(-)} \Phi_f^N | T_U^{SN} | \Phi_i^N \boldsymbol{k}_i^{(+)} \rangle + \delta_{f,i} \langle \boldsymbol{k}_f^{(-)} | U_0 | \boldsymbol{q}_i \rangle, \quad (20)$$

where $\boldsymbol{q}$ refers to a plane wave and results of physical T-matrix elements $\langle \boldsymbol{q}_f \Phi_f^N | T^{SN} | \Phi_i^N \boldsymbol{q}_i \rangle$ must be independent of the choice of U_0. Body-frame physical T-matrix elements are transformed to the laboratory frame using standard techniques and cross sections are calculated [47]. For details of the molecular CCC method see Ref. [45].

To solve Eq. (18), $\langle \boldsymbol{k}'^{(-)} \Phi_{n'}^N | V_U^D | \Phi_n^N \boldsymbol{k}^{(\pm)} \rangle$ need to be calculated. For positron- or electron-H_2 scattering the partial-wave direct V-matrix elements are given by

$$V^{\bar{M}\Pi S}_{f L_f M_f, i L_i M_i}(k_f, k_i) = \frac{2}{\pi} \delta_{\bar{M}',\bar{M}} \delta_{\Pi',\Pi} \delta_{S',S} \delta_{s',s} \sum_{\alpha\beta\gamma\delta} C^{(n')}_{\alpha,\beta} C^{(n)}_{\gamma,\delta} \delta_{l_\beta,l_\delta} \delta_{m_\beta,m_\delta} \int_0^\infty dr_2 \varphi_\beta(r_2) \varphi_\delta(r_2) \sum_{\lambda\mu} (-1)^{\lambda+\mu} C^{L0}_{L'0,\lambda 0} C^{L'M'}_{LM,\lambda-\mu}$$
$$\times \Bigg(\delta_{\mu,0} \delta_{l_\alpha,l_\gamma} \delta_{m_\alpha,m_\gamma} \int_0^\infty dr_1 \varphi_\alpha(r_1) \varphi_\gamma(r_1) \int_0^\infty dr_0 (u_{L'}(r_0;k') u_L(r_0;k) \{ z_e [1 + (-1)^\lambda] v_\lambda(r_0, R/2)$$
$$- \delta_{\lambda,0} U(r_0) \}) - 2 z_e (-1)^\lambda C^{l_\gamma 0}_{l_\alpha 0,\lambda 0} C^{l_\alpha m_\alpha}_{l_\gamma m_\gamma,\lambda\mu} \int dr_0 dr_1 [u_{L'}(r_0;k') \varphi_\alpha(r_1) v_\lambda(r_0,r_1) u_L(r_0;k) \varphi_\gamma(r_1)] \Bigg). \quad (21)$$

Here the target states of H_2 are represented by the form of Eq. (10).

The optional short-range distorting potential for H_2 is chosen as

$$U_0 = 2 z_e v_0(r_0, R/2) - 2 z_e \int d\boldsymbol{r} |\Phi_n(\boldsymbol{r})|^2 v_0(r_0, r_1), \quad (22)$$

where $\boldsymbol{r}$ is collectively all target electronic spatial coordinates, n is typically the electronic ground state, and $v_0(r_0,r_1)$ is defined as part of Eq. (5). Equation (22) utilizes the antisymmetrization property of the target states. This form of U_0 is spherically symmetric, short ranged, and ensures that the V-matrix elements are short ranged by removing the projectile-nuclei term V_0 for the $\lambda = 0$ partial wave [referring to Eq. (5)]. The use of a distorting potential is a purely numerical technique that saves on computational resources when solving the Lippmann-Schwinger equation (18) [45].

III. RESULTS

A. Scattering calculation details

The H_2 structure model needs to allow for an expansion over the two electrons (nlm,$n'l'm'$). One-electron orbitals are constructed from a Laguerre basis that has $l_{max} = 8$, $N_l = 17 - l$ functions for $l \leqslant 7$ and $N_{l=8} = 10$ with exponential falloffs $\alpha_l = 1.2$ for $l \leqslant 4$ and $\alpha_l = 1.0$ for $l \geqslant 5$. In the frozen-core model, the inner electron of H_2 is restricted to the $1s\sigma_g$ orbital of H_2^+ and the two-electron configurations have the form ($1s\sigma$,$n'l'm'$). This model is not sufficiently accurate to obtain the ground-state energy. Instead, a more accurate model is chosen with the inner and outer electrons expanded by all $n \leqslant 3$ one-electron orbitals that are constructed from short-range Laguerre basis functions with exponential falloffs of $\alpha_l = 1.9$. In addition, the $1s\sigma_g$ orbital ($n = n' = 1$) is represented by a converged molecular orbital of H_2^+ that was constructed from a Laguerre basis that had $N_l = 60 - l$, $\alpha_l = 1.7$ functions up to $l_{max} = 8$. Two-electron configurations with $|m_T| \geqslant 2$ are restricted to the frozen-core model ($1s\sigma$,$n'l'm'$), where $m_T = m + m'$. Hence the largest angular momentum projection of the states is $m_{max} = l_{max} = 8$.

Diagonalizing the target Hamiltonian with two-electron configurations built from the above model generated $N = 1013$ target states. This 1013-state model is used in the scattering calculations of positron collisions with H_2 in the $v_i = 0$ and $v_i = 1$ vibrational states. The $v = 1$ vibrational wave function approximately spans the range $0.8 \leqslant R \leqslant 2.2$. In Tables I and II the H_2 electronic states two-electron energies and ground-state static dipole polarizability are presented as a function of R. At the equilibrium distance of $R_0 = 1.4$, the static dipole polarizabilities of this model are $\alpha_\parallel = 6.375$ and $\alpha_\perp = 4.635$ for the ground state, which are both in good agreement with the accurate calculations of Kolos and Wolniewicz [48] ($\alpha_\parallel = 6.380$ and $\alpha_\perp = 4.578$). As R

TABLE I. Two-electron energies of the H_2 electronic target states $X\,^1\Sigma_g^+$, $B\,^1\Sigma_u^+$, and $C\,^1\Pi_u$ as a function of the internuclear distances R. Comparisons are made with the accurate calculations of Kolos *et al.* [49] and Wolniewicz and Dressler [51]. All values are in atomic units.

	$X\,^1\Sigma_g^+$		$B\,^1\Sigma_u^+$		$C\,^1\Pi_u$	
R	Present	[49]	Present	[51]	Present	[51]
0[a]	−2.899	−2.903	−2.123	−2.133	−2.123	−2.133
0.8	−1.015	−1.020	−0.430		−0.425	
1.0	−1.120	−1.125	−0.579	−0.581	−0.571	−0.573
1.2	−1.160	−1.165	−0.658	−0.661	−0.646	−0.649
1.4	−1.169	−1.174	−0.702	−0.706	−0.686	−0.689
1.6	−1.163	−1.169	−0.725	−0.731	−0.705	−0.709
1.8	−1.147	−1.155	−0.738	−0.745	−0.713	−0.717
2.0	−1.129	−1.138	−0.743	−0.752	−0.714	−0.718
2.2	−1.108	−1.120	−0.744	−0.756	−0.711	−0.716

[a]This entry is the combined nuclear limit of H_2, which omits the internuclear Coulomb repulsion term $1/R$ and is equivalent to atomic He. The $R = 0a_0$ energies are compared to the measurements of Moore [56] for He.

TABLE II. Parallel $\alpha_\parallel$, perpendicular $\alpha_\perp$, and total α static dipole polarizabilities of the H_2 ground state presented as a function of the internuclear distance R, compared with the accurate calculations of Kolos and Wolniewicz [48]. All values are in atomic units.

	$\alpha_\parallel$		$\alpha_\perp$		α	
R	Present	[48]	Present	[48]	Present	[48]
0[a]	1.397		1.397		1.397	1.383
0.8	3.225	3.204	2.808	2.783	2.947	2.923
1.0	4.101	4.088	3.371	3.341	3.614	3.590
1.2	5.150	5.147	3.983	3.944	4.372	4.345
1.4	6.375	6.380	4.635	4.578	5.215	5.179
1.6	7.708	7.781	5.280	5.228	6.089	6.079
1.8	9.370	9.320	6.009	5.878	7.129	7.025
2.0	11.117	10.964	6.699	6.511	8.172	7.995
2.2	13.169	12.638	7.425	7.110	9.340	8.952

[a]This entry is the combined nuclear limit of H_2, which omits the internuclear Coulomb repulsion term $1/R$ and is equivalent to atomic He. The $R = 0a_0$ polarizability is compared with the calculations of Kar and Ho [57] for He.

increases beyond the equilibrium distance of $R_0 = 1.4$, the ground and low-lying excited states of H_2 start to become more diffuse and the present structure model becomes less accurate. For the purpose of scattering calculations, the current structure model is sufficiently accurate to describe H_2 in the $v_i = 0$ and $v_i = 1$ states. Two-electron energies of the electronic excited states, vertical excitation energies, and oscillator strengths are presented for H_2 at the equilibrium internuclear distance of $R_0 = 1.4$ in Tables III and IV. These excited states are hydrogenic and are well represented in the single-center (spherical coordinate system) expansion. The present low-lying electronic excited-state energies are within 1.5% of the accurate values [49–55]. The dominant oscillator strengths are also well represented in the present model.

The present fixed-nuclei and adiabatic-nuclei results were calculated using a projectile partial-wave expansion with maximum orbital angular momentum $L_{\max} = 8$. Calculations included all possible channels (i.e., total spin $S = 1/2$, odd and

TABLE III. Two-electron energy E of the singlet ($s = 0$) electronic target states of H_2 and the vertical electronic excitation energy from the ground state ΔE at the internuclear distance $R_0 = 1.4a_0$. Comparisons are made with accurate calculations [49–54].

	E (a.u.)		ΔE (eV)	
State	Present	Ref.	Present	Ref.
$X\,^1\Sigma^+_g$	−1.169	−1.174 [49]		
$B\,^1\Sigma^+_u$	−0.702	−0.706 [51]	12.71	12.75 [51]
$EF\,^1\Sigma_g{}^+$	−0.689	−0.692 [50]	13.05	13.13 [50]
$C\,^1\Pi_u$	−0.686	−0.689 [51]	13.14	13.22 [51]
$B'\,^1\Sigma_u{}^+$	−0.627	−0.629 [51]	14.75	14.85 [51]
$GK\,^1\Sigma_g{}^+$	−0.625	−0.626 [50]	14.80	14.91 [50]
$I\,^1\Pi_g$	−0.625	−0.626 [54]	14.81	14.92 [54]
$J\,^1\Delta_g$	−0.624	−0.625 [53]	14.83	14.94 [53]
$H\,^1\Sigma_g$	−0.623	−0.624 [52]	14.86	14.97 [52]
$D\,^1\Pi_u$	−0.622	−0.624 [51]	14.88	14.99 [51]

TABLE IV. Oscillator strengths for transitions from the ground state to the lowest-lying $^1\Sigma^+_u$ and $^1\Pi_u$ states of H_2 at the internuclear distance $R_0 = 1.4a_0$. Comparisons are made with the calculations of Wolniewicz and Staszewska [55,58,59].

Transition	Length	Velocity	Refs. [55,58,59]
$X\,^1\Sigma_g{}^+ \rightarrow B\,^1\Sigma_u{}^+$	0.293	0.288	0.301
$X\,^1\Sigma_g{}^+ \rightarrow C\,^1\Pi_u$	0.354	0.351	0.358
$X\,^1\Sigma_g{}^+ \rightarrow B'\,^1\Sigma_u{}^+$	0.058	0.057	0.058
$X\,^1\Sigma_g{}^+ \rightarrow D\,^1\Pi_u$	0.087	0.086	0.085

even parity Π) up to the maximum total orbital angular momentum projection $\bar{M}_{\max} = 8$, where $-\bar{M}_{\max} \leqslant \bar{M} \leqslant \bar{M}_{\max}$. An orientationally averaged analytic Born subtraction (ABS) method was used to augment the partial-wave expansion for inelastic scattering (see Ref. [45] for details). In Sec. III C the convergence of the present partial-wave expansion is demonstrated.

In the fixed-nuclei calculation the internuclear distance was chosen as the mean internuclear distance of the H_2 vibrational ground state ($R_m = 1.448$), which approximates scattering from the vibrational ground state more accurately than the equilibrium distance ($R_0 = 1.4$) [60]. This is explicitly demonstrated in Fig. 7, which we will describe later. The dotted vertical lines at 8.6 and 15.4 eV in the figures respectively indicate the Ps formation and ionization thresholds of H_2 in the ground state. Note that with the present $R_m = 1.448$ fixed-nuclei structure model, the Ps-formation and ionization thresholds are at 9.34 and 16.14 eV, respectively.

In Ref. [61] we gave a detailed discussion of convergence studies within the (atomic and molecular) CCC method and demonstrated convergence (accurate to within numerical accuracy approximately less than 5%) of the present $R_m = 1.448$ fixed-nuclei results. Note that fixed-nuclei approximation has its own associated uncertainty, which we do not account for. Here we provide a brief discussion of our convergence studies and refer the reader to Ref. [61] for the full details.

B. Convergence with the number of states

To investigate convergence with respect to the number of states, the 1013-state model is compared with 694- and 884-state fixed-nuclei calculations. The basis used to construct the 694-state calculation was the same as the 1013-state model, however the outer electron orbitals were constructed from Laguerre basis functions that had maximum orbital angular momentum $l_{\max} = 6$. The 884-state model was produced with the same basis as the 1013-state model, except the outer electron orbitals were constructed with $N_l = 15 - l$, $l_{\max} = 8$ Laguerre basis functions. The 694-, 884-, and 1013-state GTCS and TICS are presented in Figs. 1 and 2, respectively. These results are practically the same and hence the 1013-state calculations are converged in the close-coupling expansion for both the number of Laguerre basis functions N_l and maximum orbital angular momentum $l_{\max}$ of the basis. The convergence of the 694- and 1013-state calculations indicates that the $l_{\max} = 6$ basis functions are sufficiently accurate enough to describe the long-range correlations and (virtual) Ps formation (in the low-energy region and) above the ionization threshold.

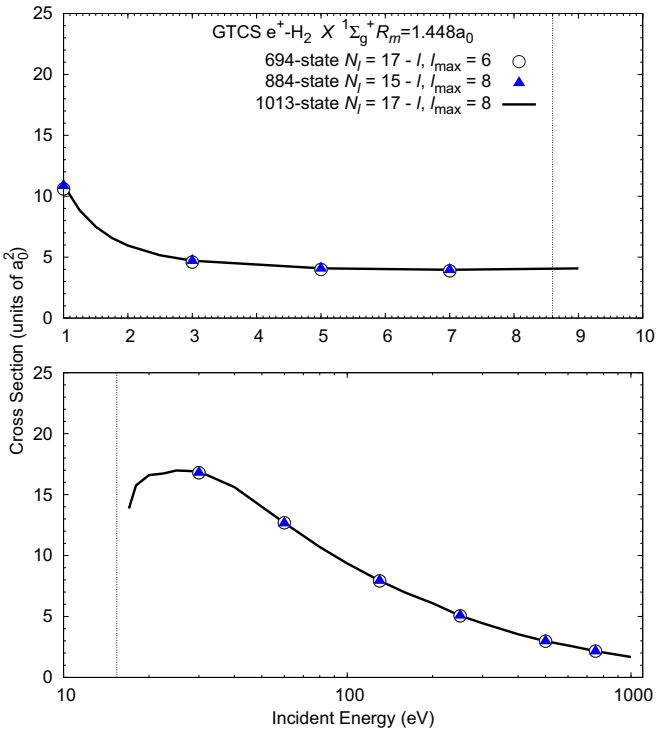

FIG. 1. Convergence studies of positron scattering from H_2 at the mean vibrational ground-state fixed-nuclei distance $R_m = 1.448a_0$. The 694-, 884-, and 1013-state CCC calculations are presented for the GTCS. A Laguerre basis with N_l functions for each orbital angular momentum l up to l_{max} is used to construct the outer electron orbitals. The dotted vertical lines at 8.6 and 15.4 eV indicate the positronium-formation and ionization thresholds of H_2 in the ground state.

Note that the sharp rise in the TICS just above the ionization threshold is from the Ps formation and direct ionization flux captured by the newly open positive-energy pseudostates. Hence a larger close-coupling calculation is expected to have a sharper TICS rise just above the ionization threshold.

To further justify that we have indeed achieved convergence with respect to the number of target states, we compare in Fig. 3 the present 1013-state calculations at the internuclear distance of $R_0 = 1.4$ with our preliminary 556-, 396-, and 276-state calculations [42]. These preliminary calculations had a completely different structure model in both N_l and the exponential falloffs α_l of the Laguerre basis functions. Hence, in the two largest models, the excited states of the discrete spectrum and the discretization of the continuum are very different. For example, in the present 1013-state model 57 states are in the discrete spectrum, while for the 556-state model ten states are in the discrete spectrum. Both $l_{max} = 8$ results are practically the same and are within 2% of the $l_{max} = 6$ results. The $l_{max} = 8$ and $l_{max} = 6$ calculations are 10% larger than the $l_{max} = 4$ results. If the $l_{max} = 8$ and $l_{max} = 6$ calculations were not converged we would expect a similar difference in magnitude between them like the case for the $l_{max} = 4$ results. Hence the 1013-, 556-, and 396-state results are converged, even though the preliminary (396- and 556-state) calculations are half the size of the 1013-state close-coupling expansion. The CCC results presented from here on are calculated with the 1013-state model.

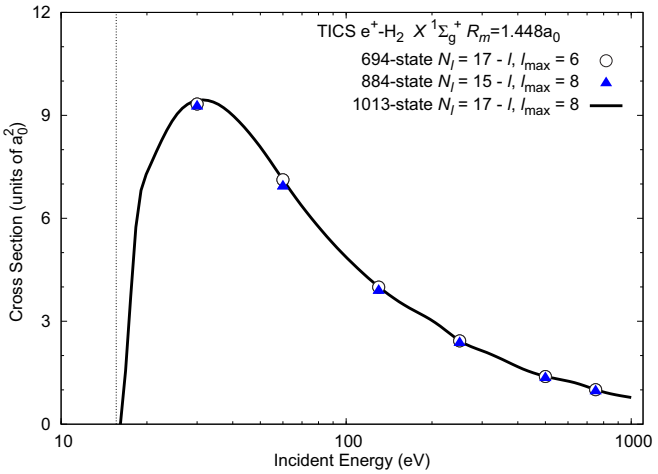

FIG. 2. Convergence studies of positron scattering from H_2 at the mean vibrational ground-state fixed-nuclei distance $R_m = 1.448a_0$. The 694-, 884-, and 1013-state CCC calculations are presented for the TICS. A Laguerre basis with N_l functions for each orbital angular momentum l up to l_{max} is used to construct the outer electron orbitals. The dotted vertical line at 15.4 eV indicates the ionization threshold of H_2 in the ground state.

C. Convergence of the partial-wave expansion

Convergence of the GTCS and TICS is investigated in Figs. 4 and 5 with respect to the size of the projectile partial-wave expansion. The 1013-state calculations were performed for partial-wave expansions with $L_{max} = \bar{M}_{max} = 7$, $L_{max} = \bar{M}_{max} = 8$, and $L_{max} = \bar{M}_{max} = 9$, which were then augmented using the ABS method. The largest difference between the $L_{max} = \bar{M}_{max} = 7$ and $L_{max} = \bar{M}_{max} = 9$ results is less than 4% at the TICS peak. The $L_{max} = \bar{M}_{max} = 8$ and

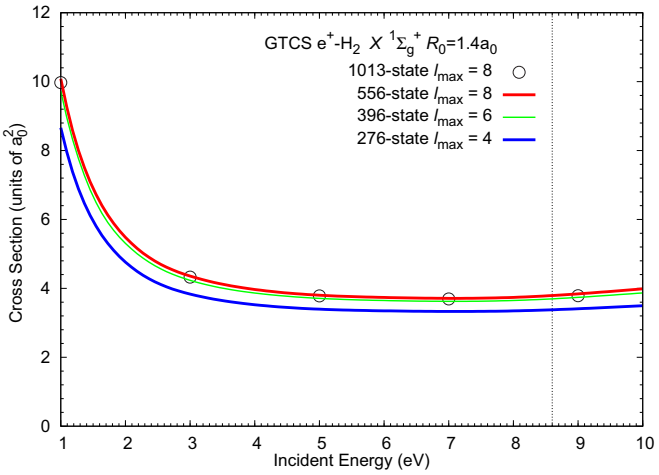

FIG. 3. Convergence studies of positron scattering from H_2 for the GTCS at the equilibrium fixed-nuclei distance $R_0 = 1.4a_0$. The present 1013-state CCC calculations are compared with the preliminary CCC calculations [42]. A Laguerre basis with orbital angular momentum l up to l_{max} is used to construct the outer electron orbitals. The dotted vertical line at 8.6 eV indicates the positronium-formation threshold of H_2 in the ground state.

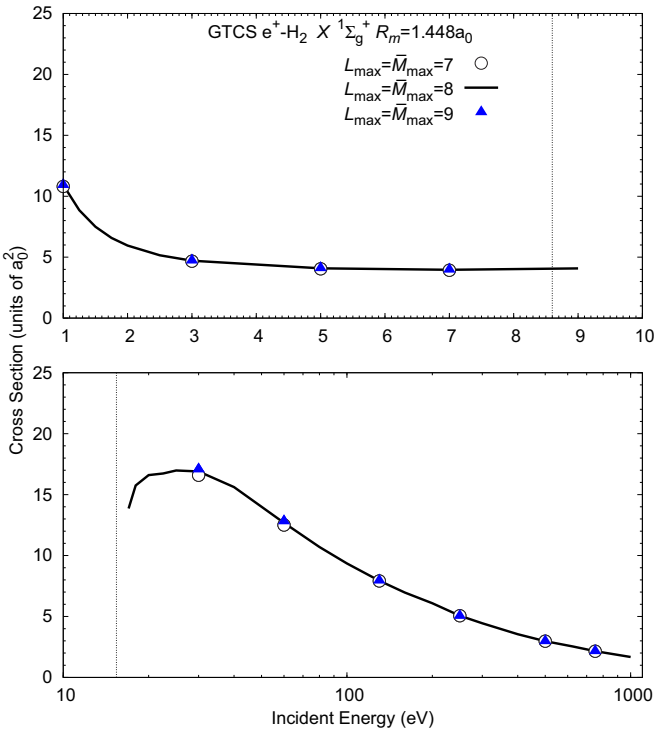

FIG. 4. Convergence studies of the GTCS for positron scattering from H_2 at the mean vibrational ground-state fixed-nuclei distance $R_m = 1.448a_0$. The 1013-state CCC results are calculated using a partial-wave expansion with maximum orbital angular momentum $L_{\max}$ and maximum total orbital angular projection $\bar{M}_{\max}$. An orientationally averaged analytic Born subtraction method is used to augment results. The dotted vertical lines at 8.6 and 15.4 eV indicate the positronium-formation and ionization thresholds of H_2 in the ground state.

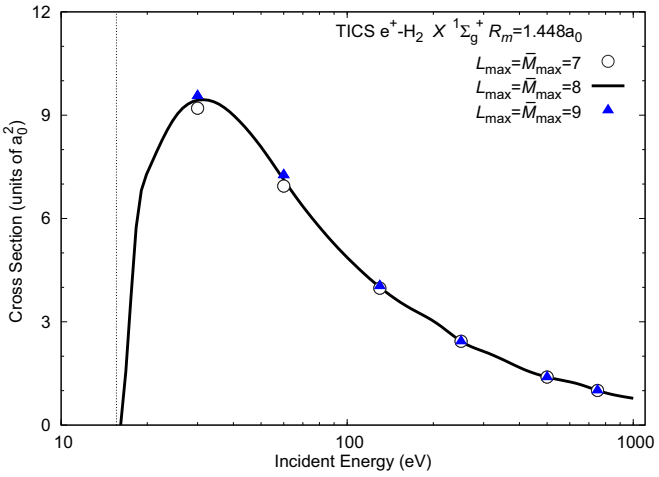

FIG. 5. Convergence studies of the TICS for positron scattering from H_2 at the mean vibrational ground-state fixed-nuclei distance $R_m = 1.448a_0$. The 1013-state CCC results are calculated using a partial-wave expansion with maximum orbital angular momentum $L_{\max}$ and maximum total orbital angular projection $\bar{M}_{\max}$. An orientationally averaged analytic Born subtraction method is used to augment results. The dotted vertical line at 15.4 eV indicates the ionization threshold of H_2 in the ground state.

$L_{\max} = \bar{M}_{\max} = 9$ TICS and GTCS are practically the same across the entire energy range and are therefore converged.

Hence the 1013-state CCC results presented here are converged in both the projectile partial-wave and close-coupling expansions. From here on the presented results have been calculated using the 1013-state model and a partial-wave expansion with maximum orbital angular momentum and maximum total orbital angular projection $L_{\max} = \bar{M}_{\max} = 8$. Convergence studies suggest that the present fixed-nuclei $R_m = 1.448$ 1013-state CCC results are estimated to be accurate to within 5% for the GTCS and TICS. This accuracy estimate does not include the uncertainty associated with the fixed-nuclei approximation.

D. Scattering length of the ground and first vibrationally excited states

The adiabatic-nuclei integrated cross section for a transition $i, v_i \rightarrow f, v_f$ is defined as [47]

$$\sigma^S_{f v_f, i v_i} = \frac{q_f}{q_i} \frac{1}{4\pi} \sum_{\substack{L_f, L_i \\ M_f, M_i}} \left| \langle v_f v_f | A^{S(\mathrm{b})}_{f L_f M_f, i L_i M_i} | v_i v_i \rangle_R \right|^2, \quad (23)$$

where the transition is from an initial electronic state i and vibrational state v_i to a final electronic state f and vibrational state v_f, $v_{i v_i}(R)$ is the vibrational wave function,

$$A^{S(\mathrm{b})}_{f L_f M_f, i L_i M_i}(R) = -(2\pi)^2 (q_f q_i)^{-1} i^{L_i - L_f} \times T^{S(\mathrm{b})}_{f L_f M_f, i L_i M_i}(q_f, q_i; R), \quad (24)$$

the superscript (b) indicates the body-frame, and the physical T-matrix elements $T^{S(\mathrm{b})}_{f L_f M_f, i L_i M_i}(q_f, q_i; R)$ are from the physical T matrix with the form given in Eq. (19). The vibrational wave functions only have a minor dependence on the rotational quantum number J and hence it can be assumed that they are independent of J. Here we chose $J = 0$ and the vibrational wave functions were calculated with the same method described in Ref. [45], however here we utilized the accurate H_2 ground-state Born-Oppenheimer potential energy curve calculated by Kolos *et al.* [49].

The 1013-state CCC calculations described above in Sec. III A were conducted at eight internuclear points within the interval $0.8 \leqslant R \leqslant 2.2$. The real and imaginary parts of the T-matrix elements were found to be smooth as a function of R and were interpolated separately over this interval.

To investigate the accuracy of the adiabatic-nuclei CCC results, calculations were performed at sufficiently low energies to calculate the scattering length A, where

$$\sigma(0) = 4\pi A^2, \quad (25)$$

with $\sigma(0)$ the GTCS at 0 eV [62]. The CCC scattering lengths are compared with the accurate calculations of Zhang *et al.* [60,63] as a function of R in Fig. 6. At $R_m = 1.448$ the CCC calculations obtain a scattering length of $A = -2.65$, which compares very well with the accurate result of $A = -2.71$ [60]. The CCC results are also in excellent agreement with the calculations of Zhang *et al.* [60,63] in the interval $0.8 \leqslant R \leqslant 2.0$. This excellent agreement indicates that the current CCC calculations model virtual

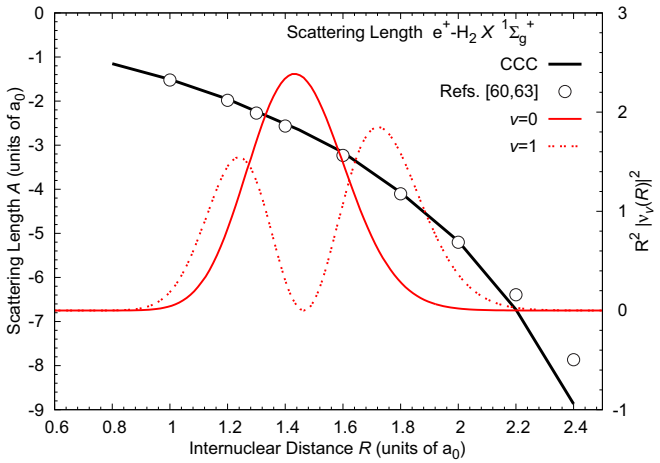

FIG. 6. Scattering length A of positron scattering from the electronic ground state of H_2 presented as a function of the internuclear distance R. Convergent close-coupling results are compared with the results of Zhang *et al.* [60,63]. The red lines are the vibrational probability density functions $R^2|v_v(R)|^2$ of the H_2 electronic ground $v = 0$ and $v = 1$ vibrational states.

Ps formation sufficiently accurately. At $R = 2.2$ there is a difference of approximately 5% between the CCC results and the calculations of Zhang *et al.* [60,63]. This difference comes from the choice of the structure (1013-state) model, where the low-lying excited states of H_2 start to become more diffuse and the present structure model becomes less accurate. As shown in Fig. 6, this interval approximately spans the range of the H_2 $v = 0$ and $v = 1$ vibrational state probability density functions. Adiabatic-nuclei results for scattering from the electronic ground $v_i = 0$ and $v_i = 1$ vibrational states of H_2 only have a minor contribution from T-matrix elements [Eq. (23)] or cross sections $\sigma_{f,i}(R)$ [Eq. (26)] for $R \geqslant 2.2$. Referring to Fig. 6, this is because the respective vibrational wave functions are very small at these values of R.

Calculating the adiabatic-nuclei GTCS at (near) zero incident energy with Eq. (23) for the ground $v_i = 0$ and first vibrationally excited $v_i = 1$ states, we can obtain the scattering length of H_2 in the $v_i = 0$ and $v_i = 1$ states with Eq. (25). This calculation gives the $v_i = 1$ scattering length as $A = -3.16$, which is 17% larger than the $v_i = 0$ scattering length of $A = -2.70$.

E. Scattering from the ground and first vibrationally excited states

Summing over all final vibrational state transitions in Eq. (23) by utilizing the closure property of the complete vibrational basis, the integrated cross section for the transition $i, v_i \rightarrow f$ is calculated with

$$\sigma^S_{f,iv_i} = \int R^2 dR\, \sigma^S_{f,i}(R) \left| v_{iv_i}(R) \right|^2, \tag{26}$$

where $\sigma^S_{f,i}(R)$ is the fixed-nuclei integrated cross section at the internuclear distance R [45,47]. The 1013-state CCC calculations described above were conducted at eight internuclear points within the interval $0.8 \leqslant R \leqslant 2.2$. Cross sections were found to be smooth as a function of R and were interpolated

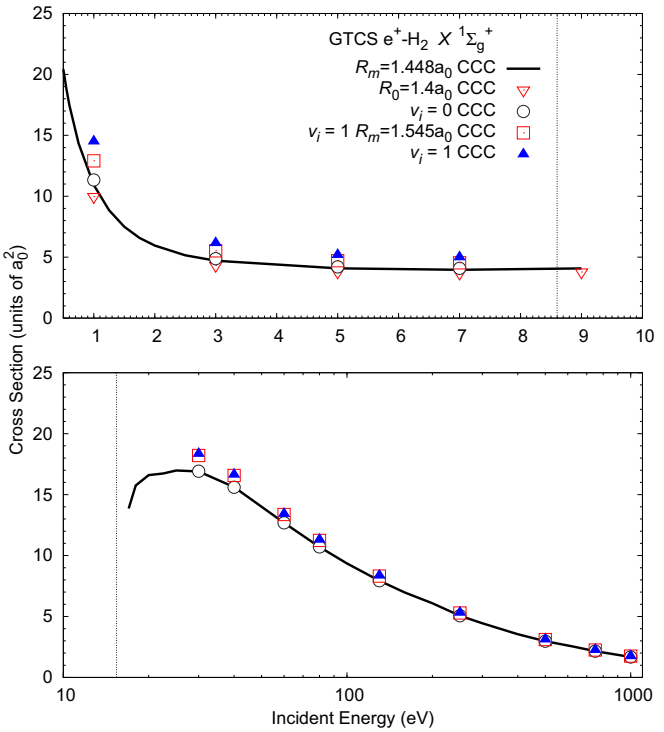

FIG. 7. Grand total cross section for positron scattering from the $v_i = 0$ and $v_i = 1$ vibrational states of H_2. Adiabatic-nuclei CCC results are compared with the fixed-nuclei CCC calculations at the mean internuclear distances of the $v_i = 0$ state ($R_m = 1.448a_0$), the $v_i = 1$ state ($R_m = 1.545a_0$), and the equilibrium ($R_0 = 1.4a_0$) distance. The dash-dotted vertical lines at 8.6 and 15.4 eV indicate the positronium-formation and ionization thresholds of H_2 in the ground state.

in this interval of R. Using Eq. (26), adiabatic-nuclei results are presented for positron scattering from the electronic ground $v_i = 0$ and $v_i = 1$ vibrational states of H_2. It is important to note that in the fixed-nuclei and adiabatic-nuclei approximations (26), the closure method is used to analytically sum over all final vibrational and rotational excitations.

The 1013-state adiabatic-nuclei and fixed-nuclei GTCS are presented in Fig. 7 for positron scattering from the $v_i = 0$ and $v_i = 1$ states of H_2. In the low-energy region (1–10 eV) the adiabatic-nuclei $v_i = 1$ results are between 20% and 30% larger than the $v_i = 0$ results. This significant difference between the $v_i = 0$ and $v_i = 1$ cross sections is likely to be important in transport models [1,2]. Above the ionization threshold the $v_i = 1$ results are at most 10% larger than the $v_i = 0$ results. As the incident projectile energy increases the $v_i = 0$ and $v_i = 1$ cross sections converge and by 250 eV results are practically the same.

Comparing the adiabatic-nuclei $v_i = 0$ results and the fixed-nuclei mean internuclear distance $R_m = 1.448$ results, we find that the cross sections are practically the same. In the energy range presented here the largest difference is approximately 3% (in the low-energy region). Note that in the low-energy region the adiabatic-nuclei $v_i = 0$ results are 5%–15% larger than the equilibrium $R_0 = 1.4$ fixed-nuclei results. This confirms that for fixed-nuclei calculations the mean internuclear distance is a better approximation of $v_i = 0$

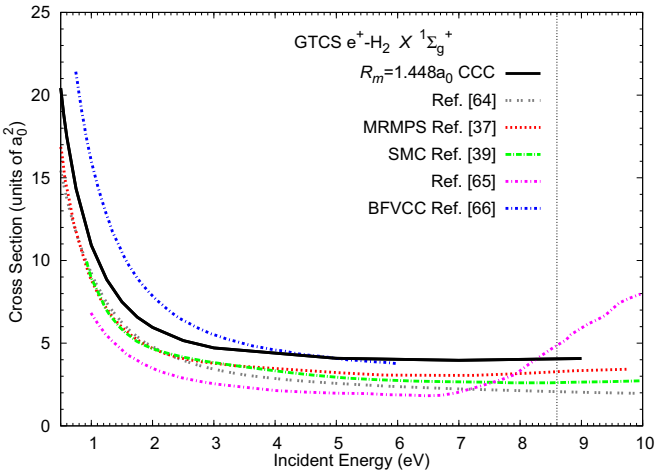

FIG. 8. Grand total cross section for positron scattering from the ground state of H_2. The mean internuclear distance $R_m = 1.448a_0$ fixed-nuclei CCC results are compared with equilibrium $R_0 = 1.4a_0$ fixed-nuclei results from the method of continued-fraction calculation of Tenfen *et al.* [64], the MRMPS calculations of Zhang *et al.* [37], the SMC calculations of Sanchez and Lima [39], and the first-order method of Reid *et al.* [65]. Results are also compared with the BFVCC calculations of Gianturco and Mukherjee [66]. The dash-dotted vertical line at 8.6 eV indicates the positronium-formation threshold of H_2 in the ground state.

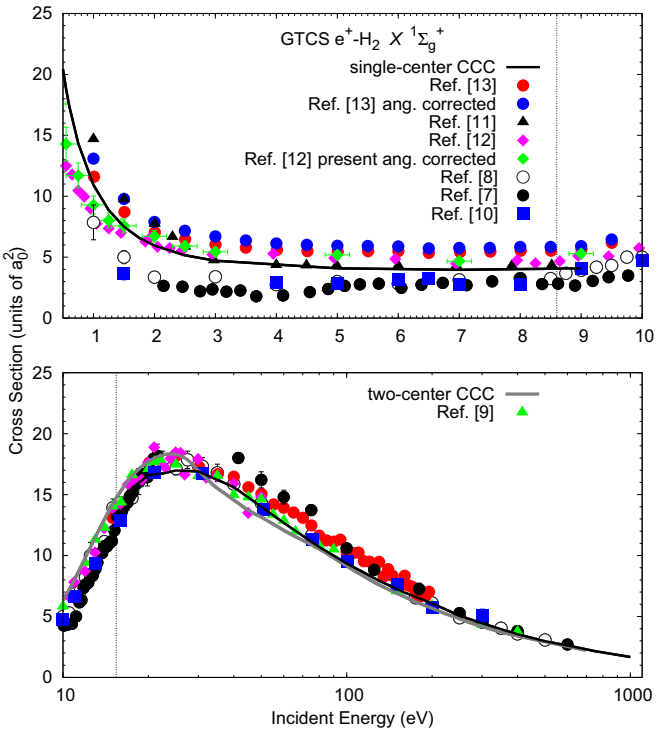

FIG. 9. Convergent close-coupling results of the GTCS for positron scattering from the ground state of H_2. The mean internuclear distance $R_m = 1.448a_0$ fixed-nuclei single-center CCC results (present) are compared with the two-center CCC calculations [32] and the measurements of Machacek *et al.* [13], Karwasz *et al.* [11], Zecca *et al.* [12], Hoffman *et al.* [8], Charlton *et al.* [7], Zhou *et al.* [10], and Deuring *et al.* [9]. The dash-dotted vertical lines at 8.6 and 15.4 eV indicate the positronium-formation and ionization thresholds of H_2 in the ground state.

than the equilibrium distance. The fixed-nuclei cross sections taken (from interpolated values) at the mean internuclear distance of the first excited vibrational state $R_m = 1.545$ are compared with the $v_i = 1$ adiabatic-nuclei results. Above the ionization threshold the mean fixed-nuclei results look to be a good approximation of the adiabatic-nuclei results, where cross sections at high energies have less of a dependence on R than low-energy cross sections. At low energies there is a significant difference, where the $v_i = 1$ adiabatic-nuclei results are about 10% larger than the $R_m = 1.545$ results. We expect that using the mean internuclear distance to approximate scattering from vibrational levels will be a worse approximation for higher excited vibrational levels.

The low-energy GTCS is presented in Fig. 8 for positron scattering from the ground state of H_2. Fixed-nuclei $R_m = 1.448$ CCC results are compared with equilibrium distance $R_0 = 1.4$ fixed-nuclei theoretical results calculated with the continued fractions method of Tenfen *et al.* [64], the MRMPS method of Zhang *et al.* [37], the SMC method of Sanchez and Lima [39], and the first-order (*ad hoc*) method of Reid *et al.* [65]. It is important to note that the fixed-nuclei $R_m = 1.448$ CCC results are 5%–15% larger than the $R_0 = 1.4$ CCC results. There is still, however, a large variation between fixed-nuclei single-center close-coupling method (CCC, MRMPS, and SMC) results, where CCC results are 20%–30% larger than the MRMPS and SMC results. The variation in these results comes primarily from the different-size close-coupling expansions utilized in the respective calculations. The SMC and MRMPS calculations utilize basis expansions that have $l_{\max} = 3$ and $l_{\max} = 5$, respectively. Noting that the CCC calculations utilize a basis expansion with $l_{\max} = 8$ suggests that the SMC and MRMPS calculations have not modeled virtual Ps formation to convergence. As an additional check $R_0 = 1.4$ CCC calculations were performed with the same-size basis as the MRMPS calculations [37]; these CCC and MRMPS results were almost identical. The present CCC results are also in good agreement with the body-frame vibrational close-coupling (BFVCC) calculations of Gianturco and Mukherjee [66] above 4 eV. It is interesting to note that all theoretical results have the same qualitative behavior except for the results of Reid *et al.* [65] near the Ps-formation threshold.

In Fig. 9 the GTCS is compared with experiments for positron scattering from the ground state of H_2. Fixed-nuclei $R_m = 1.448$ CCC results are compared with the measurements of Machacek *et al.* [13], Karwasz *et al.* [11], Zecca *et al.* [12], Hoffman *et al.* [8], Charlton *et al.* [7], Zhou *et al.* [10], and Deuring *et al.* [9]. Machacek *et al.* [13] have also corrected their low-energy measurements to account for scattering to forward angles. In the low-energy region experimental results show large variations. These variations are primarily due to different experimental resolution of scattering to forward angles [12,13]. The angular resolutions of the Zecca *et al.* [12], Karwasz *et al.* [11], and Machacek *et al.* [13] experiments are the most superior [12,67]. The experiments of Hoffman *et al.* [8], Charlton *et al.* [7], Zhou *et al.* [10], and Deuring *et al.* [9] may have missed a significant fraction of scattering to forward angles and therefore measured lower

TABLE V. Grand total cross section for positron scattering from the ground state of H_2. The present low-energy measurements of Zecca *et al.* [12], corrected to account for scattering to forward angles, are compared with the present CCC results.

Energy (eV)	Corrected GTCS (10^{-16} cm^2)	CCC GTCS (10^{-16} cm^2)
0.10	12.52 ± 1.50	14.44
0.20	7.74 ± 0.87	10.58
0.35	4.92 ± 0.51	7.49
0.55	4.00 ± 0.38	5.27
0.75	3.28 ± 0.29	4.02
1.00	2.60 ± 0.21	3.06
1.25	2.25 ± 0.17	2.48
1.50	2.12 ± 0.16	2.10
2.00	1.88 ± 0.14	1.67
2.50	1.65 ± 0.11	1.44
3.00	1.52 ± 0.10	1.32
5.00	1.45 ± 0.09	1.14
7.00	1.31 ± 0.08	1.11
9.00	1.48 ± 0.08	1.14

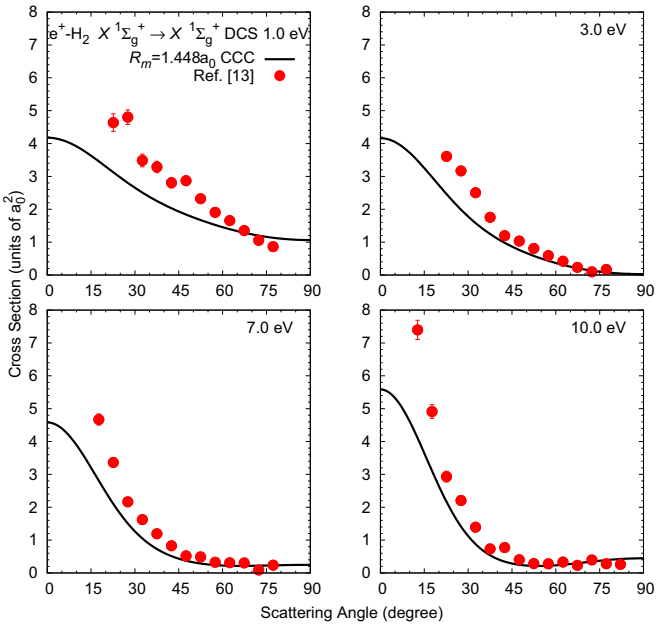

FIG. 10. The 1.0-, 3.0-, 7.0-, and 10-eV elastic (summed over all vibrational and rotational excitations) DCSs for positron scattering from the ground state of H_2. The mean internuclear distance $R_m = 1.448a_0$ fixed-nuclei CCC results and the measurements of Machacek *et al.* [13] have summed the DCS at θ and $180^\circ - \theta$.

cross sections [12]. For example, at 5 eV the measurements of Machacek *et al.* [13] had an angular resolution of $\sim 10^\circ$, while the experiment of Hoffman *et al.* [8] had an angular resolution of $\sim 25^\circ$. Note that the angular resolution of a measurement is dependent on the projectile, target, and incident energy [8]. The CCC results are in the best agreement with the measurements of Zecca *et al.* [12] and Karwasz *et al.* [11].

The present low-energy measurements of Zecca *et al.* [12] corrected to account for scattering to forward angles are also shown in Fig. 9 (top panel) and listed in numerical form in Table V. That correction has been calculated following the method described by Hamada and Sueoka [68] and using the present CCC elastic differential cross sections (analytically summed over all vibrational and rotational excitations) in conjunction with the energy-dependent angular discrimination θ_c of the Trento spectrometer [69]. Briefly, the forward-angle-scattering correction was calculated as follows:

$$\sigma_T^{\rm corr} = \sigma_T^{\rm uncorr}/(1 - C), \tag{27}$$

where $\sigma_T^{\rm corr}$ and $\sigma_T^{\rm uncorr}$ are the corrected and uncorrected GTCS, respectively, and the correction factor C is given by

$$C = \frac{\int_0^{\theta_c} \frac{d\sigma}{d\Omega} \sin(\theta) d\theta}{\int_0^{\pi} \frac{d\sigma}{d\Omega} \sin(\theta) d\theta}. \tag{28}$$

After the correction for forward scattering, the experimental GTCS of Zecca *et al.* [12] increase between $\sim 20\%$ at the lowest energies and $\sim 3\%$ at 9 eV. Above 10 eV that correction has not been applied as it is expected to be smaller than 3% and therefore lies well within the experimental uncertainties. Even though the measurements of Zecca *et al.* [12] have been corrected with the present CCC results, there is still a considerable discrepancy between theory and experiment below 1 eV. This might be explained, at least in part, by the convolution of the measured GTCS over the finite-energy distribution of the incident positron beam. The overall uncertainty on the experimental energy scale of the positron beam (± 0.2 eV) might also play a role. We recall here that this stems from both the uncertainty on the calibration of the energy scale (± 0.05 eV) and the energy spread of the positron beam (~ 0.12 eV full width at half maximum). On the theoretical side, we also mention that at these low energies coupling to nuclear motion may be important.

Above the ionization threshold (bottom panel of Fig. 9) all experiments [7–10,12,13] are in good agreement with each other and the single-center CCC results. The good agreement with experiment at the cross-section maximum (25 eV) suggests that the 1013-state CCC calculations are sufficiently converged to model Ps formation. The two-center CCC method [32] utilized an approximation in the rearrangement matrix elements, approximating the positron-nuclei potential as isotropic. Unfortunately, testing internal consistency between the single- and two-center CCC calculations is not feasible in the low- and intermediate-energy range, where this approximation is expected to break down. However, we find that the two calculations are within reasonable agreement with each other in the intermediate-energy region and converge at higher energies as expected.

It is interesting to note that the GTCS measurements of Machacek *et al.* [13] are consistently higher than other experiments [8–10] and the single- and two-center CCC results at low and high energies. At these high energies Ps formation is negligible and the experimental forward-angle-scattering effect should not be an issue.

Low-energy elastic DCSs are presented in Fig. 10. The experiment of Machacek *et al.* [13] measured the electronic elastic cross section summed over all final vibrational and rotational transitions. Note that fixed-nuclei DCS and integrated

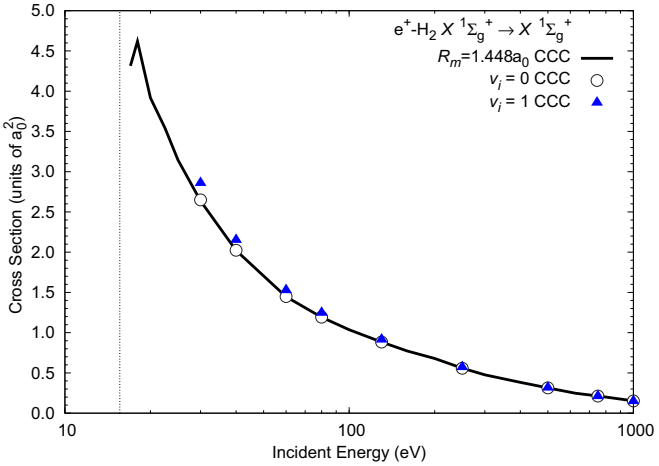

FIG. 11. Convergent close-coupling results of the elastic (summed over all vibrational and rotational excitations) integrated cross section for positron scattering from the $v_i = 0$ and $v_i = 1$ vibrational states of H_2. The mean internuclear distance $R_m = 1.448a_0$ fixed-nuclei results are compared with the adiabatic-nuclei results. The dash-dotted vertical line at 15.4 eV indicates the ionization threshold of H_2 in the ground state.

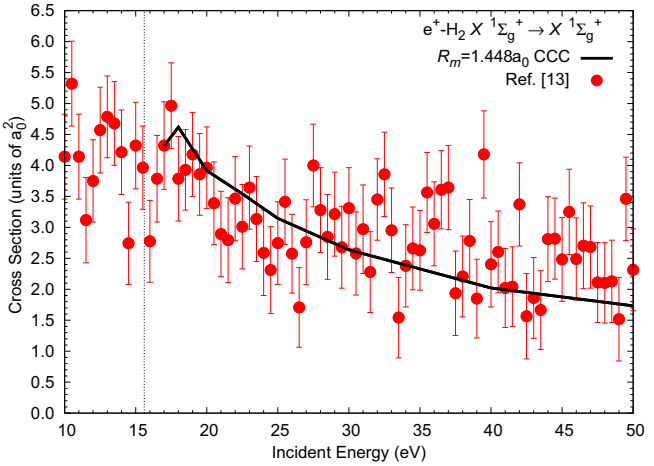

FIG. 12. Convergent close-coupling results of the elastic (summed over all vibrational and rotational excitations) integrated cross section for positron scattering from the ground state of H_2. The mean internuclear distance $R_m = 1.448a_0$ fixed-nuclei results are compared with the measurements of Machacek *et al.* [13]. The dash-dotted vertical line at 15.4 eV indicates the ionization threshold of H_2 in the ground state.

cross sections are analytically summed over all vibrational and rotational excitations [47] and hence describe the same process as measured in the experiment [13]. The experiment of Machacek *et al.* [13] also sums measurements of the DCS at θ and $180^\circ - \theta$. Here the CCC results are combined in the same way to compare with the experiment. The CCC results are in good qualitative agreement with the 3.0, 7.0, and 10 eV measured DCSs but underestimate experimental measurements in the forward (and backward) scattering angles. For the 1 eV DCS, CCC results do not agree with the shape or magnitude of the measurements. The rapid rise of the GTCS around 1 eV (see Fig. 8) is possibly a contributing factor. However, even taking into account the uncertainty estimates of the present fixed-nuclei CCC results, there is still a significant difference between theory and experiment at the forward-scattering angles. As shown in Secs. III B and III C, the fixed-nuclei CCC results are converged in both the close-coupling and partial-wave expansions and are also in excellent agreement with the scattering length results of Zhang *et al.* [60,63]. Hence these calculations can only be improved by coupling to vibrational and rotational degrees of freedom.

The adiabatic-nuclei CCC elastic (summed over all vibrational and rotational excitations) integrated cross section is presented in Fig. 11 for positron scattering from the $v_i = 0$ and $v_i = 1$ vibrational states of H_2. Comparing the fixed-nuclei $R_m = 1.448$ and adiabatic-nuclei $v_i = 0$ results, we find that the cross sections are practically the same. The difference between the $v_i = 0$ and $v_i = 1$ results is relatively minor, where the $v_i = 1$ cross section is at most 10% larger than the $v_i = 0$ results.

The $R_m = 1.448$ fixed-nuclei CCC elastic (summed over all vibrational and rotational excitations) integrated cross section is compared with the corresponding measurements of Machacek *et al.* [13] in Fig. 12 for H_2 in the $v_i = 0$ state. As a consequence of distinguishing between the elastic and inelastic scattering processes, the elastic measurements of Machacek *et al.* [13] missed a larger portion of forward-angle scattering compared to the measurements of the GTCS. These measurements are expected to rise when scattering to forward angles is accounted for. Given the large variation and uncertainty in the measurements, it is difficult to draw any solid conclusions regarding the comparison with theory. The CCC results are however within the uncertainties of almost all experimental points.

The adiabatic-nuclei TICS of positron scattering from the $v_i = 0$ and $v_i = 1$ vibrational states is presented in Fig. 13. The

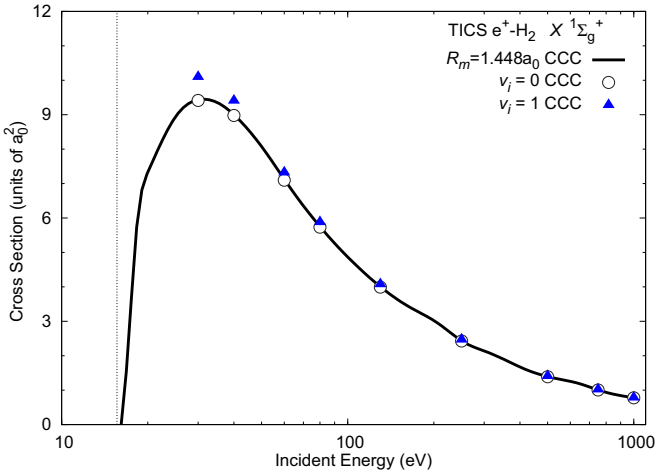

FIG. 13. Total ionization cross section for positron scattering from the $v_i = 0$ and $v_i = 1$ vibrational states of H_2. Adiabatic-nuclei CCC results are compared with the mean internuclear distance $R_m = 1.448a_0$ fixed-nuclei calculations. The dash-dotted vertical line at 15.4 eV indicates the ionization threshold of H_2 in the ground state.

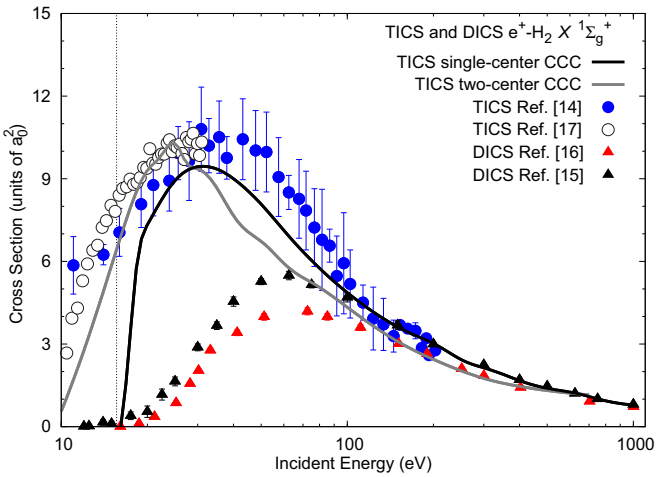

FIG. 14. Convergent close-coupling results of the TICS for positron scattering from the ground state of H_2. The mean internuclear distance $R_m = 1.448a_0$ single-center CCC (present) TICSs are compared with the $R_0 = 1.4a_0$ two-center CCC TICSs [32], the measurements of Fromme *et al.* [14] and Moxom *et al.* [17], and the DICSs measured by Jacobsen *et al.* [16] and Knudsen *et al.* [15]. The dash-dotted vertical line at 15.4 eV indicates the ionization threshold of H_2 in the ground state.

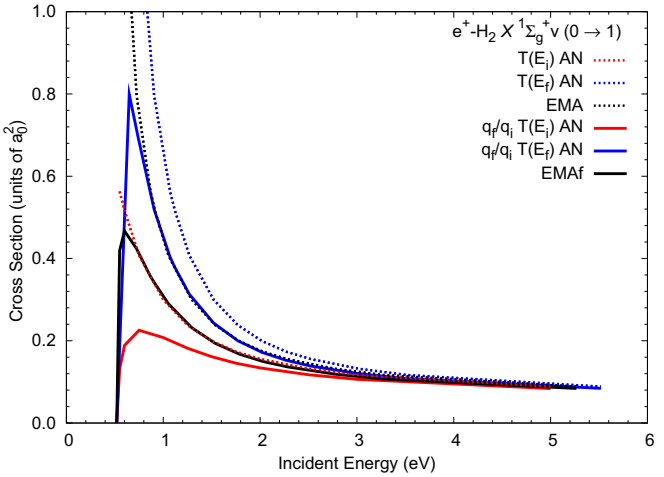

FIG. 15. Positron scattering from the ground state of H_2 for the $0 \rightarrow 1$ vibrational excitation cross section. Refer to the text for details of the present models.

$v_i = 1$ state TICS is noticeably larger than the $v_i = 0$ results in the intermediate-energy region. The largest difference is at the peak of the cross section (at 30 eV), where the $v_i = 1$ TICS is approximately 7% larger than the $v_i = 0$ TICS. Again, the $v_i = 1$ results converge to the $v_i = 0$ results at larger energies, about 130 eV. Comparing the $v_i = 0$ and the fixed-nuclei $R_m = 1.448$ calculations, results are practically the same over the entire energy range.

The $R_m = 1.448$ single-center CCC TICS is compared with the measurements of Fromme *et al.* [14] and Moxom *et al.* [17] and the $R_0 = 1.4$ two-center CCC TICS [32] in Fig. 14. The TICS maximum at approximately 30 eV has the largest contribution from the Ps-formation cross section compared to the DICS, which is measured by Jacobsen *et al.* [16] and Knudsen *et al.* [15].

Comparing the single- and two-center CCC results, in the intermediate-energy range the results vary significantly, while at higher energies there is good agreement between the two calculations. This difference could be due to the two-center CCC calculations approximating the positron-molecule potential as spherical, which is a good approximation at high impact energies. The good agreement at the cross-section maximum between the single-center CCC TICS and the TICS measurements of Fromme *et al.* [14] and Moxom *et al.* [17] suggests that the 1013-state CCC calculations have a sufficiently large close-coupling expansion to indirectly model Ps formation. As the projectile energy increases the Ps-formation cross section diminishes and becomes negligible at approximately 130 eV [13]. Above 130 eV the CCC TICS can be compared with the DICS measurements of Jacobsen *et al.* [16] and Knudsen *et al.* [15]. Here the single-center CCC results are in good agreement with both experiments but favor the measurements of Knudsen *et al.* [15].

F. Vibrational excitation cross section

The vibrational excitation cross section calculated within the adiabatic-nuclei approximation [refer Eq. (23)] violates the conservation of energy law (due to a vibrational transition). Mazevet *et al.* [70] have investigated several adiabatic-nuclei energy correction methods by comparing vibrational close-coupling cross sections with adiabatic-nuclei energy-corrected cross sections in e-H_2 scattering. They concluded that the relatively simple energy-modified adiabatic phase matrix (EMAP) method produces reasonably accurate vibrational excitation cross sections at energies away from threshold and nonadiabatic resonances. For very accurate excitation cross sections near threshold, the first-order nondegenerate adiabatic approximation method is better suited; it retains energy conservation and produces results with the correct threshold behavior. The energy-corrected adiabatic nuclear vibration method (referred to as ANVf in their paper) is calculated simply with the adiabatic-nuclei cross section (23) but with a corrected flux factor q_f/q_i so as to force the cross section to zero at threshold by having $q_f = \sqrt{2[E_i - (\varepsilon_{f,v_f} - \varepsilon_{i,v_i})]}$, where $E_i = q_i^2/2$ and ε_{n,v_n} is the energy of the n electronic and v_n vibrational state. We assume here that $J = 0$ for all states.

In Fig. 15 we compare several adiabatic-nuclei correction methods for the $0 \rightarrow 1$ vibrational excitation cross section in positron-H_2 scattering. The first method is the adiabatic-nuclei (AN) cross section [Eq. (23)] without the corrected flux factor, i.e., $q_f/q_i = 1$, which is indicated in the figures by $T(E_i)$ AN. For electronically elastic transitions it is unclear whether to use the fixed-nuclei T matrix at the incident energy $T(E_i)$ or the fixed-nuclei T matrix at the (corrected) outgoing energy $T(E_f)$ [71], where $E_f = q_f^2/2$. Here we also investigate having $T(E_f)$, indicated in the figures by $T(E_f)$ AN. The third method we have used is the energy-modified adiabatic (EMA) approximation first proposed by Nesbet [72]. Here the electronically elastic fixed-nuclei T matrix is set as $T(E_{\rm EMA})$, where $E_{\rm EMA} = \sqrt{E_i E_f}$ is the geometric mean of the incident E_i and outgoing energy E_f. This approximation is appropriate to account for vibrational excitations that obey

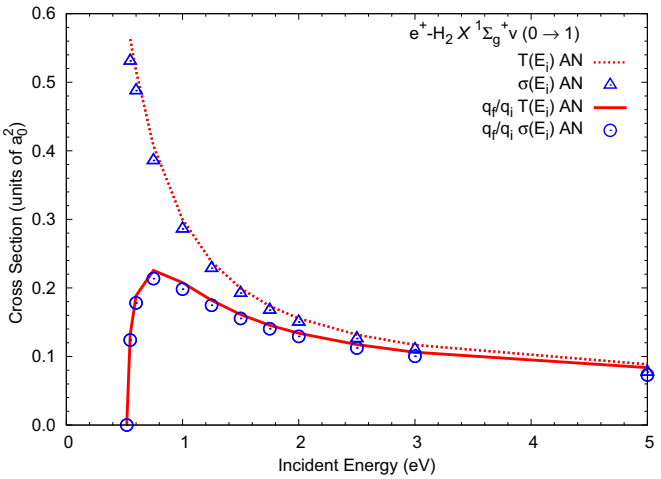

FIG. 16. Positron scattering from the ground state of H_2 for the $0 \rightarrow 1$ vibrational excitation cross section. Refer to the text for details of the present models.

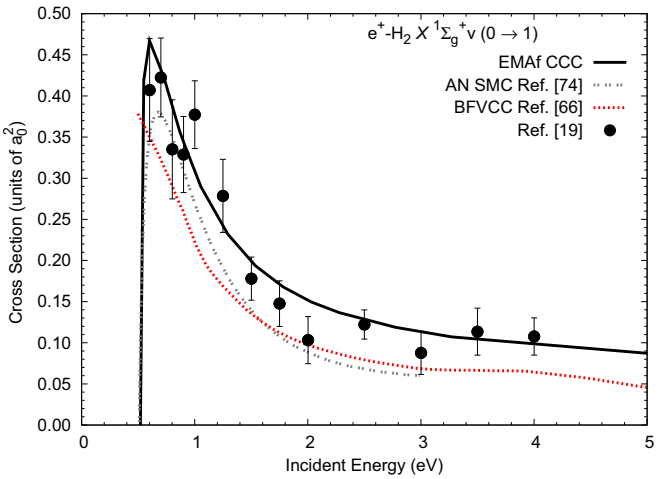

FIG. 17. Positron scattering from the ground state of H_2 for the $0 \rightarrow 1$ vibrational excitation cross section. The EMAf-corrected CCC results are compared with the AN SMC calculations of Varella and Lima [74], the BFVCC calculations of Gianturco and Mukherjee [66], and the measurements of Sullivan *et al.* [19].

the short-range interaction threshold law, but loses its validity for long-range potentials and under conditions where vibronic interactions are strong [70]. Similar to the EMAP method, the EMA method applies the energy shift to the (S or) T matrix, while the EMAP method applies the energy shift to the K matrix in order to enforce unitarity to the T matrix. The EMAf method indicates that the adiabatic-nuclei cross section in Eq. (23) is calculated with $T(E_{\rm EMA})$ and the corrected flux factor. Other calculations that include the corrected flux factor are indicated by q_f/q_i.

Turning to Fig. 15 we compare the $T(E_i)$ AN and $T(E_f)$ AN cross sections. The qualitative behavior between the two results is identical, however the $T(E_f)$ AN results are shifted towards the higher energies relative to the $T(E_i)$ AN results. The EMA method is between these two results. These cross sections however do not go to zero at threshold [as we are using electronic elastic T-matrix elements in Eq. (23)] unless they include the corrected flux factor. Surprisingly, the EMAf method is practically identical to the (uncorrected) $T(E_i)$ AN results just after threshold. All these adiabatic-nuclei correction methods obtain the same results at higher energies.

A series of experiments on electron-molecular ion scattering [73] utilizes an approximation of the adiabatic-nuclei cross section to analyze their results such that

$$\sigma_{f v_f, i v_i} \approx |\langle \nu_{f v_f} | \sqrt{\sigma_{f,i}(R)} | \nu_{i v_i} \rangle_R|^2. \tag{29}$$

We note that utilizing Eq. (29) is significantly simpler and computationally more efficient than using Eq. (23). In Fig. 16 we present the approximation of Eq. (29) [indicated by $\sigma(E_i)$ in the figure], as well as the correction methods mentioned above. Comparing the $T(E_i)$ AN results and those calculated with the approximation of Eq. (29), the results are surprisingly practically identical.

The CCC EMAf results are compared with the adiabatic-nuclei SMC projection-operator calculations of Varella and Lima [74], the BFVCC calculations of Gianturco and Mukherjee [66], and the measurements of Sullivan *et al.* [19] in Fig. 17. The present CCC EMAf results are in excellent agreement with experiment in both the shape and magnitude of the cross section. The CCC EMAf shape results are in good agreement with the adiabatic-nuclei SMC projection-operator results [74] and BFVCC results [66], but are systematically higher with a difference at 3 eV of about 80%. This is not due to the present correction method chosen here, as all the correction method results are practically identical above 3.5 eV (as seen from Figs. 15 and 16). It is also important to note that the adiabatic-nuclei SMC projection-operator results [74] are based on fixed-nuclei calculations that use a much smaller basis ($l_{\rm max} = 1$) than the present calculations ($l_{\rm max} = 8$). Such a basis size [74] will produce fixed-nuclei results that are significantly unconverged, as indicated in Fig. 3.

IV. CONCLUSION

The single-center CCC method has been applied to positron scattering from H_2 in the electronic ground $v_i = 0$ and $v_i = 1$ vibrational states. The reasonably large difference between results for scattering from the $v_i = 0$ and $v_i = 1$ vibrational states indicates that inclusion of these processes may be important in transport modeling. Results were presented for the scattering length and the elastic scattering, total ionization, vibrational excitation, and grand total cross sections. In addition, the present elastic DCSs were used to correct the low-energy GTCS measurements of Zecca *et al.* [12] for the forward-angle-scattering effect. Here the fixed-nuclei CCC calculations explicitly demonstrate convergence in the close-coupling (target-state) and projectile partial-wave expansions. We estimate that the major integrated cross sections are accurate to within $\pm 5\%$ in the fixed-nuclei approximation. In general, comparison with experiment is good.

However, there is still some discrepancy between the CCC results and recent low-energy measurements of the GTCS [12,13]. This is surprising as we have explicitly

demonstrated convergence and the fixed-nuclei (ground state) scattering length obtained here ($A = -2.65a_0$) is in excellent agreement with accurate calculations [60,63] ($A = -2.71a_0$). We also found that the GTCS is in excellent agreement with measurements in the intermediate-energy region, which indicates that calculations have accurately accounted for Ps formation. In addition, the present EMAf $0 \rightarrow 1$ vibrational excitation cross section is calculated from the low-energy GTCS and is in excellent agreement with the experiment of Sullivan *et al.* [19]. This serves as an independent check in support of our GTCS. We are confident in the accuracy of the EMAf method as the basis of this method (EMAP) worked very well when applied to electron-H_2 scattering [70]. Hence calculations can only rigorously be improved by coupling electronic and nuclei motion. However, at these energies (4–8 eV) this coupling is not expected to play a significant role.

In the future we are planning to investigate the positron-H_2 electronic and rotational excitations. Our long term goal is to extend the single-centre CCC method to positron scattering from arbitrary diatomic molecules.

ACKNOWLEDGMENTS

This work was supported by the United States Air Force Office of Scientific Research, Los Alamos National Laboratory (LANL), and Curtin University. M.C.Z. would like to specifically acknowledge LANL's ASC PEM Atomic Physics Project for its support. The LANL is operated by Los Alamos National Security, LLC for the National Nuclear Security Administration of the U.S. Department of Energy under Contract No. DEAC52-06NA25396. Resources were provided by the Pawsey Supercomputing Centre with funding from the Australian Government and the Government of Western Australia.

[1] R. White, W. Tattersall, G. Boyle, R. Robson, S. Dujko, Z. Petrovic, A. Bankovic, M. Brunger, J. Sullivan, S. Buckman *et al.*, Appl. Radiat. Isotopes **83**, 77 (2014).
[2] G. J. Boyle, W. J. Tattersall, D. G. Cocks, S. Dujko, and R. D. White, Phys. Rev. A **91**, 052710 (2015).
[3] V. Cobut, Y. Frongillo, J. P. Patau, T. Goulet, M.-J. Fraser, and J.-P. Jay-Gerin, Radiat. Phys. Chem. **51**, 229 (1998).
[4] I. Baccarelli, I. Bald, F. A. Gianturco, E. Illenberger, and J. Kopyra, Phys. Rep. **508**, 1 (2011).
[5] B. Boudaïffa, P. Cloutier, D. Hunting, M. A. Huels, and L. Sanche, Science **287**, 1658 (2000).
[6] N. Guessoum, Eur. Phys. J. D **68**, 1 (2014).
[7] M. Charlton, T. C. Griffith, G. R. Heyland, and G. L. Wright, J. Phys. B **13**, L353 (1980).
[8] K. R. Hoffman, M. S. Dababneh, Y. F. Hsieh, W. E. Kauppila, V. Pol, J. H. Smart, and T. S. Stein, Phys. Rev. A **25**, 1393 (1982).
[9] A. Deuring, K. Floeder, D. Fromme, W. Raith, A. Schwab, G. Sinapius, P. W. Zitzewitz, and J. Krug, J. Phys. B **16**, 1633 (1983).
[10] S. Zhou, H. Li, W. E. Kauppila, C. K. Kwan, and T. S. Stein, Phys. Rev. A **55**, 361 (1997).
[11] G. P. Karwasz, D. Pliszka, and R. S. Brusa, Nucl. Instrum. Methods Phys. Res. Sect. B **247**, 68 (2006).
[12] A. Zecca, L. Chiari, A. Sarkar, K. L. Nixon, and M. J. Brunger, Phys. Rev. A **80**, 032702 (2009).
[13] J. R. Machacek, E. K. Anderson, C. Makochekanwa, S. J. Buckman, and J. P. Sullivan, Phys. Rev. A **88**, 042715 (2013).
[14] D. Fromme, G. Kruse, W. Raith, and G. Sinapius, J. Phys. B **21**, L261 (1988).
[15] H. Knudsen, L. Brun-Nielsen, M. Charlton, and M. R. Poulsen, J. Phys. B **23**, 3955 (1990).
[16] F. M. Jacobsen, N. P. Frandsen, H. Knudsen, and U. Mikkelsen, J. Phys. B **28**, 4675 (1995).
[17] J. Moxom, G. Laricchia, and M. Charlton, J. Phys. B **26**, L367 (1993).
[18] J. P. Sullivan, J. P. Marler, S. J. Gilbert, S. J. Buckman, and C. M. Surko, Phys. Rev. Lett. **87**, 073201 (2001).
[19] J. P. Sullivan, S. J. Gilbert, J. P. Marler, L. D. Barnes, S. J. Buckman, and C. M. Surko, Nucl. Instrum. Methods Phys. Res. Sect. B **192**, 3 (2002).
[20] J. P. Sullivan, C. Makochekanwa, A. Jones, P. Caradonna, D. S. Slaughter, J. Machacek, R. P. McEachran, D. W. Mueller, and S. J. Buckman, J. Phys. B **44**, 035201 (2011).
[21] A. C. L. Jones, C. Makochekanwa, P. Caradonna, D. S. Slaughter, J. R. Machacek, R. P. McEachran, J. P. Sullivan, S. J. Buckman, A. D. Stauffer, I. Bray *et al.*, Phys. Rev. A **83**, 032701 (2011).
[22] J. P. Sullivan, C. Makochekanwa, A. Jones, P. Caradonna, and S. J. Buckman, J. Phys. B **41**, 081001 (2008).
[23] J. Tennyson, Phys. Rep. **491**, 29 (2010).
[24] N. R. Hewitt, C. J. Noble, and B. H. Bransden, J. Phys. B **23**, 4185 (1990).
[25] N. R. Hewitt, C. J. Noble, and B. H. Bransden, J. Phys. B **25**, 557 (1992).
[26] K. Higgins and P. G. Burke, J. Phys. B **24**, L343 (1991).
[27] J. Mitroy, Aust. J. Phys. **46**, 751 (1993).
[28] H. R. J. Walters, A. A. Kernoghan, M. T. McAlinden, and C. P. Campbell, in *Photon and Electron Collisions with Atoms and Molecules*, edited by P. G. Burke and C. J. Joachain (Plenum, New York, 1997), pp. 313–345.
[29] A. S. Kadyrov and I. Bray, Phys. Rev. A **66**, 012710 (2002).
[30] R. Utamuratov, A. S. Kadyrov, D. V. Fursa, I. Bray, and A. T. Stelbovics, J. Phys. B **43**, 125203 (2010).
[31] A. V. Lugovskoy, A. S. Kadyrov, I. Bray, and A. T. Stelbovics, Phys. Rev. A **82**, 062708 (2010).
[32] R. Utamuratov, A. S. Kadyrov, D. V. Fursa, M. C. Zammit, and I. Bray, Phys. Rev. A **92**, 032707 (2015).
[33] A. S. Kadyrov and I. Bray, J. Phys. B **49**, 222002 (2016).
[34] I. Bray, D. V. Fursa, A. S, Kadyrov, A. V. Lugovskoy, J. S. Savage, A. T. Stelbovics, R. Utamuratov, and M. C. Zammit, J. Phys.: Conf. Ser. **488**, 012052 (2014).
[35] P. K. Biswas, J. S. E. Germano, and T. Frederico, J. Phys. B **35**, L409 (2002).
[36] I. Bray, J. J. Bailey, D. V. Fursa, A. S. Kadyrov, and R. Utamuratov, Eur. Phys. J. D **70**, 1 (2016).
[37] R. Zhang, K. L. Baluja, J. Franz, and J. Tennyson, J. Phys. B **44**, 035203 (2011).
[38] F. Arretche and M. A. P. Lima, Phys. Rev. A **74**, 042713 (2006).
[39] S. d. A. Sanchez and M. A. P. Lima, Nucl. Instrum. Methods Phys. Res. Sect. B **266**, 447 (2008).

[40] J. N. Cooper, E. A. G. Armour, and M. Plummer, J. Phys. B **41**, 245201 (2008).
[41] M. Charlton, T. C. Griffith, G. R. Heyland, and G. L. Wright, J. Phys. B **16**, 323 (1983).
[42] M. C. Zammit, D. V. Fursa, and I. Bray, Phys. Rev. A **87**, 020701 (2013).
[43] J. T. Broad and W. P. Reinhardt, J. Phys. B **9**, 1491 (1976).
[44] M. C. Zammit, D. V. Fursa, and I. Bray, Phys. Rev. A **88**, 062709 (2013).
[45] M. C. Zammit, D. V. Fursa, and I. Bray, Phys. Rev. A **90**, 022711 (2014).
[46] M. C. Zammit, J. S. Savage, D. V. Fursa, and I. Bray, Phys. Rev. Lett. **116**, 233201 (2016).
[47] N. F. Lane, Rev. Mod. Phys. **52**, 29 (1980).
[48] W. Kolos and L. Wolniewicz, J. Chem. Phys. **46**, 1426 (1967).
[49] W. Kolos, K. Szalewicz, and H. J. Monkhorst, J. Chem. Phys. **84**, 3278 (1986).
[50] J. W. Liu and S. Hagstrom, Phys. Rev. A **48**, 166 (1993).
[51] L. Wolniewicz and K. Dressler, J. Chem. Phys. **88**, 3861 (1988).
[52] L. Wolniewicz and K. Dressler, J. Chem. Phys. **100**, 444 (1994).
[53] L. Wolniewicz, J. Mol. Spectrosc. **174**, 132 (1995).
[54] L. Wolniewicz, J. Mol. Spectrosc. **169**, 329 (1995).
[55] L. Wolniewiczi, Wolniewiczi molecular hydrogen database, http://fizyka.umk.pl/ftp/pub/publications/ifiz/luwo/.
[56] C. E. Moore, *Atomic Energy Levels as Derived from Analyses of Optical Spectra*, Natl. Bur. Stand. (U.S.) Circ. No. 467 (U.S. GPO, Washington, DC, 1949), Vol. 1.
[57] S. Kar and Y. K. Ho, J. Quant. Spectrosc. Radiat. Transfer **109**, 445 (2008).
[58] L. Wolniewicz and G. Staszewska, J. Mol. Spectrosc. **217**, 181 (2003).
[59] L. Wolniewicz, Chem. Phys. Lett. **233**, 644 (1995).
[60] J. Y. Zhang and J. Mitroy, Phys. Rev. A **83**, 022711 (2011).
[61] M. C. Zammit, D. V. Fursa, and I. Bray, J. Phys.: Conf. Ser. **635**, 012009 (2015).
[62] B. H. Bransden, *Atomic Collision Theory*, 2nd ed. (Benjamin/Cummings, Reading, 1983).
[63] J.-Y. Zhang, J. Mitroy, and K. Varga, Phys. Rev. Lett. **103**, 223202 (2009).
[64] W. Tenfen, K. T. Mazon, S. E. Michelin, and F. Arretche, Phys. Rev. A **86**, 042706 (2012).
[65] D. D. Reid, W. B. Klann, and J. M. Wadehra, Phys. Rev. A **70**, 062714 (2004).
[66] F. A. Gianturco and T. Mukherjee, Phys. Rev. A **64**, 024703 (2001).
[67] K. Fedus, J. Franz, and G. P. Karwasz, Phys. Rev. A **91**, 062701 (2015).
[68] A. Hamada and O. Sueoka, J. Phys. B **27**, 5055 (1994).
[69] A. Zecca, L. Chiari, A. Sarkar, and M. J. Brunger, New J. Phys. **13**, 115001 (2011).
[70] S. Mazevet, M. A. Morrison, O. Boydstun, and R. K. Nesbet, J. Phys. B **32**, 1269 (1999).
[71] Y. Itikawa and N. Mason, Phys. Rep. **414**, 1 (2005).
[72] R. K. Nesbet, Phys. Rev. A **19**, 551 (1979).
[73] M. O. A. E. Ghazaly, J. Jureta, X. Urbain, and P. Defrance, J. Phys. B **37**, 2467 (2004).
[74] M. T. d. N. Varella and M. A. P. Lima, Phys. Rev. A **76**, 052701 (2007).